The Astrophysical Journal, 736:152 (8pp), 2011 August 1 doi:10.1088/0004-637X/736/2/152

MODELING OF THE INITIAL MASS FUNCTION USING THE METROPOLIS–HASTINGS ALGORITHM

Tanuka Chattopadhyay[1], Asis Kumar Chattopadhyay[2], and Abisa Sinha[2]
[1] Department of Applied Mathematics, Calcutta University, 92 A.P.C. Road, Kolkata 700009, India; tanuka@iucaa.ernet.in
[2] Department of Statistics, Calcutta University, 35 B.C. Road, Kolkata 700019, India; akcstat@caluniv.ac.in
Received 2011 February 12; accepted 2011 May 15; published 2011 July 19

ABSTRACT

A stochastic model has been developed for the hierarchical fragmentation of a molecular cloud. Here, the number of fragments, time between successive fragmentation steps, and mass of a fragment are considered as random variables, and fragment masses are generated using the Metropolis–Hastings algorithm. The resulting mass spectra, computed at different projected distances and taking opacity into consideration, show a signature of mass segregation. The critical mass, mass spectrum, and mass segregation are consistent with the observations of young massive clusters in our Galaxy as well as in external galaxies.

Key words: methods: statistical – stars: luminosity function, mass function

1. INTRODUCTION

The initial mass function (IMF) is a measure of the mass spectrum of stars in different environments, e.g., field, stellar association, open clusters, globular clusters (GCs), young massive clusters (YMCs). It was first introduced by Salpeter (1955) and is a power law of the form $\xi = dN/d\log m \propto m^{\Gamma}$, where m is the mass of a star and N is the number of stars in the logarithmic mass ranges $\log m$ and $(\log m + d\log m)$. It was found that $\Gamma \sim -1.35$ for $0.4\,M_{\odot} \leqslant m \leqslant 10\,M_{\odot}$. The IMF in linear mass units takes the form $dN/dm \propto m^{-\alpha}$ so that $\Gamma = \alpha - 1$. Later, a segmented power law was derived (Kroupa et al. 1993) that gave $\Gamma \sim -1.35$ above a few solar masses, with a shallower power law ($\Gamma \sim 0$ to -0.25) for low-mass stars. The turnover occurs at $0.3\,M_{\odot}$, often known as the characteristic mass (m_c). Thus, anomalies exist in the shape of the mass spectrum in the low-mass regime. YMCs, which are dense aggregates of young stars, have received considerable attention since the 1960s (Hodge 1961). The planar distribution of open clusters, YMCs, and GCs in the Milky Way is quite distinct, but in the mass–radius diagram, YMCs seem to be closely associated with GCs (Zwart et al. 2010), so they are expected to fill the gap between young and low-mass open clusters and old massive GCs in that we can expect that, after a prescribed time (∼10 Gyr), they will possess a roughly spherical structure and a surface brightness distribution similar to that of old GCs. Also, they are believed to be fundamental building blocks of galaxies. Their ages are on the order of a few Myr (∼100 Myr), and they are more massive than $\sim 10^4\,M_{\odot}$. There is observational evidence that mass segregation (Figer et al. 1999; Espinoza et al. 2009; Brandner et al. 2008; Harayama et al. 2008) results in steepening the IMF in the outer part of the cluster. The resulting mass segregation cannot be due to dynamical interaction because their ages are much shorter than their current relaxation timescale, so it is regarded as having a primordial origin.

Several works have been carried out by various authors to find the origin of such primordial mass segregation. Moeckel & Bonnell (2009) suggested that the young ages (∼Myr) of the massive clouds are responsible for the mixing of spatially distinct populations of stars, which in turn gives rise to the initial mass segregation in the parent cloud. This idea was tested using N-body simulation. Allison et al. (2009a) suggested that young massive clouds form cool clumpy substructures, which dynamically evolve in a much shorter timescale compared to that needed for typical dynamical evolution, giving rise to mass segregation. The above theory was supported by Er et al. (2009), in which a Monte Carlo simulation model was adopted for embedded clusters to study their dynamical evolution in addition to random motions of massive stars and dynamical friction from gas. A completely different cause of mass segregation was suggested by Pasquato et al. (2009), who suggested that the presence of an intermediate massive black hole in GCs is responsible for mass segregation. This theory is revealed by the measurement of the radial profile of the average mass of stars in the system. Allison et al. (2009b) applied the method of a minimum spanning tree for most massive stars and random stars to search for mass segregation in the Orion nebula. Evidence of mass segregation was found down to $0.5\,M_{\odot}$. Moeckel & Clarke (2011) investigated the accretion-driven contraction of protoclusters of various masses. They found that in low-density protoclusters, e.g., Orion, the collision is unimportant, whereas in large clouds these collisions play an important part in the early mass segregation of these clusters. Ascenso et al. (2009) studied the measure of an indicator commonly used to discern mass segregation in young stellar clusters and found that the measure is highly sensitive to the effect of incompleteness of observational data. On the other hand, Chavarría et al. (2009) showed that the mass segregation in young clusters is not due to incompleteness of observational data but rather to dynamical interactions of the cluster members with dense gas from the parent cloud.

In the above discussion, different factors were taken into account to clarify the origin of mass segregation in young massive star clusters without any robust conclusion. The actual fragmentation process is more complicated than the assumed models outlined in the above theories. On the other hand, the mass spectrum found that as a result of fragmentation a certain probability distribution follows, e.g., a power law with a steeper slope in the massive zone compared to shallower ones of varying slopes in the less-massive regime. This inspired some authors to adopt various stochastic models to better understand the origin of the IMF and mass segregation observed in YMCs.

Elmegreen & Mathieu (1983) modeled the fragmentation of molecular clouds as a random process, considering the number of fragments at each step, fractional masses of the fragments, and the number of fragmentation steps as random variables following Gaussian distributions. The resulting mass spectrum is a lognormal after only four or five fragmentation

steps, irrespective of the various initial parameter choices. In continuation, Wolf & Vanysek (1986) adopted a similar model with one additional variable, which was the chance of fragmentation as a function of fragment mass following the Cauchy distribution. The modeled mass spectrum was compared to the observed IMF of some open clusters. Fragmentation is also modeled following the probabilistic approach of Moultaka & Pelat (2004). Chattopadhyay et al. (2003) considered random fragmentation of molecular clouds and took the effect of time into account. The distribution of the number of fragments is time-dependent, and the time between successive fragmentation events is generated by a Poisson process. The resulting mass spectrum is a single power law with a slope much steeper than the Salpeter slope.

In the above studies on random fragmentation, either time spent in successive fragmentation events is not considered or, if it is considered, the mass spectrum found is a single power law of a much steeper slope than the Salpeter slope or lognormal mass function. The observed mass spectrum is neither a single power law nor a symmetric one in the logarithm-of-mass plot, but rather a segmented power law, viz. the Salpeter slope in the high-mass region and a shallower slope in the low-mass region beyond a critical mass ($\sim 0.3\,M_{\odot}$). Moreover, in the above models, observed mass segregation was not modeled with random fragmentation. In addition, in the studies of mass segregation, the role of opacity was not discussed. Finally, the fragment mass distribution was generated by a Gaussian distribution following the argument of the central limit theorem. Collecting all theoretical models and observational facts, it is clear that the process of fragmentation and cause of mass segregation are more complicated than the models considered so far. In this work, a distribution-free approach was adopted for the fragmentation model, and random fragmentation of massive clouds was considered. The fragment masses are generated by a process rather than a hypothetical parametric distribution, and the final mass distribution found is independent of the initial choice. Generally, the assumption of a Gaussian distribution is very common because of the central limit theorem, but, it is difficult to determine the sample size that makes the sample Gaussian in nature, especially for a time-limited model in which fragmentation cannot continue for an infinitely long time and the number of fragments indefinitely increases. In this context, it should be mentioned that Elmegreen (1997) considered the fragmentation of a turbulent cloud and found the power-law mass distribution contrary to the result found in a previous paper (Elmegreen & Mathieu 1983).

The present problem demonstrates a time-dependent model of hierarchical random fragmentation of YMCs under various initial conditions. Here, the number of fragments and time between successive fragmentation events are considered to be random variables, generated by a Monte Carlo simulation using the corresponding distribution functions, whereas the fragment masses are generated by the Metropolis–Hastings algorithm, which is a Markov chain-based simulation process. Then, the mass spectra are studied at different projected distances from the cluster center, taking into consideration the opacity-limited fragmentation scenario (Kanjilal & Basu 1992), to investigate the effect of resulting mass segregation. The random fragmentation process, concept of opacity, and observations at different projected distances are simultaneously incorporated into the present model, which is a completely new approach. The resulting mass spectrum demonstrates well the observed segmented power-law form of the mass spectrum in a more or less consistent way in many YMCs in our Galaxy, as well as in external galaxies. It should be noted that in the analytical model of opacity-limited fragmentation considered by Kanjilal & Basu (1992), the mass spectrum found is also steeper than the observed Salpeter slope for high-mass fragments. In Section 2, the fragmentation scenario and resulting mass spectrum are demonstrated. Section 3 discusses the method, while Section 4 describes results and presents discussion.

2. FRAGMENTATION AND MASS DISTRIBUTION

While considering the IMF of stars, several authors (Elmegreen & Mathieu 1983; Wolf & Vadimir 1986; Larson 1973) have considered the application of the random fragmentation theory. Random fragmentation of a line into n parts and its application in assessing the randomness of radioactive disintegration and cosmic-ray events were considered by Feller (1980). Elmegreen & Mathieu (1983) studied the form of the mass spectrum by considering random fragmentation using a Monte Carlo simulation for a time-independent model suggested by Larson (1973). They assumed an initial Gaussian distribution of the number of fragments as well as their masses, but in their work, they did not introduce the effect of the time interval between two successive fragmentations, which is also a random variable. Chattopadhyay et al. (2003) considered this effect in the following manner. If a line of length l is divided at random into N_F parts, the average number of fragments will exceed the value x, given by (Feller 1980)

$$N_F \left(1 - \frac{x}{l}\right)^{N_F - 1}. \tag{1}$$

Following the above argument, if N_F is the total number of fragments formed within a given time interval t_1 (say) after a fragmentation step in the hierarchy, then the probability that the time elapsed between successive fragmentations will not exceed t is given by

$$P(t, N_F, t_1) = 1 - (1 - t/t_1)^{N_F}. \tag{2}$$

Previously, Auluck & Kothari (1965) considered only N_F to be random in the above expression, but Chattopadhyay et al. (2003) have also considered time t a random variable because the time interval between two successive fragmentations also has to be random. According to Feller (1980), the probability of the occurrence in a run of duration t of exactly n events is given by the Poisson formula

$$W_n(t) = e^{-\lambda t} \frac{(\lambda t)^n}{n!}. \tag{3}$$

Here, the distribution of inter-occurrence time is given by

$$P(t) = 1 - e^{-\lambda t}. \tag{4}$$

In the above expression, the parameter λ can be estimated by the reciprocal of the average time ($\bar{t}$) between successive fragmentations, i.e., $\hat{\lambda} = 1/\bar{t}$. The average time of fragmentation (Chattopadhyay et al. 2003) is $\bar{t} \leqslant y/n$, where y is the maximum time of successive fragmentation steps and n is the number of fragmentation steps. Further,

$$n \leqslant (\log m_f + \log m_{\min})/(\log N_F), \tag{5}$$

where m_f is the mass of the parent cloud and $m_{\min}$ is the minimum mass of a fragment. Unlike Elmegreen & Mathieu

(1983) and Chattopadhyay et al. (2003), in the present work the relative masses (m_i) of the fragments are generated using the Metropolis–Hastings algorithm by eliminating the assumption of normality. The arguments for this consideration were discussed in the Introduction.

2.1. Opacity-limited Fragmentation at Projected Distances from the Cluster Center

Opacity-limited fragmentation was considered (Kanjilal & Basu 1992) for a spherically collapsing, isothermal molecular cloud in which molecular hydrogen and grains are the only cooling and opacity sources. There, a broad spectrum of minimum Jeans mass was produced, varying from $\sim$0.002 $M_\odot$ to 0.1 $M_\odot$ depending on the type of grain and metallicity (Z) values. The minimum mass also increases if metallicity decreases; this is actually the effect of opacity. As metallicity decreases, opacity decreases; because density is proportional to opacity, density decreases, and as a result the Jeans mass increases, so the minimum Jeans mass increases as one moves from the center to the outer part of the cloud. Thus, the above variation can be considered as

$$m_{\rm min} = Ar^{\delta}, \tag{6}$$

where $m_{\rm min}$ is the minimum Jeans mass of a fragment at a distance r (three dimensional) from the center of the cloud and A and δ are constants. Observational evidence of minimum mass to support Equation (6) is not available because the distance (viz. r) considered here is three dimensional and, for YMCs and other stellar populations, we always see the projected distance of various objects. The effect of such variation when observing substellar objects at various projected distances is reflected in several works, e.g., Marsh et al. (2010), who found objects in the mass range of 2–3 Jupiter masses in the ρOph cloud core. Moreover, a theoretical model of opacity-limited fragmentation (Bate 2005) predicted that low-mass objects would be observed three times more frequently in high-metallicity compared to low-metallicity calculations. In addition, a minimum mass range on the order of 0.007–0.01 $M_\odot$ was found as a result of opacity-limited fragmentation in a three-dimensional model considered by Boyd & Whitworth (2005). Hence, we consider representative values of $m_{\rm min} = 0.04\,M_\odot$ and 0.01 $M_\odot$ at $r = 15$ pc ($r_{\rm max}$) and 1.5 pc, respectively. The number density of fragments at a distance r from the cluster center is assumed to follow a distribution of the form following the Elson–Fall–Freeman (EFF) surface brightness profile (Elson et al. 1987), with $2 < \gamma < 3$:

$$n(r) = \frac{C}{(1 + r^2/a^2)^{\gamma/2}}, \tag{7}$$

where the surface brightness is defined as the luminosity within a distance r; a is the scale parameter; and

$$r_c = a(2^{2/\gamma} - 1), \tag{8}$$

with r_c being the core radius of the cloud, defined as the distance from the cluster center at which the surface brightness drops by a factor of two from the central value. In computing the value of a used in Equation (7), the value of r_c is used via Equation (8). Then, summing $n(r_i)$, $i = 1, 2, \ldots$, max, the value of C is found, because the total number of fragments formed in a cloud of size $r_{\rm max}$ (= 15 pc) is assumed to be fixed ($\sim$10,000) in each simulation. Generating $n(r_i)$ fragments at each r_i, $i = 1, 2, \ldots$, max (Figure 1), the cumulative mass spectrum at a projected distance b from the center of the cloud can be computed. Finally, the mass spectra at different projected distances are computed to investigate the existence of mass segregation.

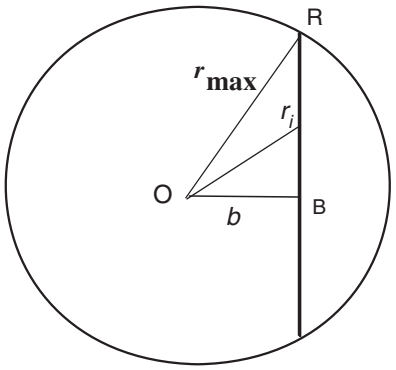

Figure 1. Schematic diagram of a YMC showing b, $r_{\rm max}$, and r_i.

3. MARKOV CHAIN MONTE CARLO SIMULATION

A Markov chain is a sequence of random variables with discrete-state space and one-step dependence. One can use an ergodic Markov chain with stationary distribution f to generate a sample, approximately distributed as f, without directly simulating from f. This is particularly useful when the nature of f is complicated; the distribution function cannot be written in closed form, direct sampling from which is difficult. A Markov Chain Monte Carlo (MCMC) method for simulating distribution f is a technique for producing an ergodic Markov chain where the stationary distribution is f. In such situations, the Metropolis–Hastings algorithm is used. The Metropolis–Hastings algorithm (Robert & Casella 1998) starts with target density $f(x)$ and proposal density $q(y|x)$, which depends on the current state $x = x^{(t)}$, to generate a new proposed sample, $y = x^{(t+1)}$. The algorithm can be implemented when it is easy to simulate from $q(.|x)$ and is either explicitly available up to a multiplicative constant independent of x or symmetric in nature. The algorithm produces a Markov chain, $X^{(t)}$, through the following steps.

1. Generate $y^t \sim q(y|x^{(t)})$.
2. Take $x^{(t+1)} = y^t$ with probability $\rho(x^{(t)}, y^t) = x^{(t)}$ with probability $1 - \rho(x^{(t)}, y^t)$ where $\rho(x, y) = \min[\frac{f(y)q(x|y)}{f(x)q(y|x)} - 1]$.

If the chain starts with a value $x^{(0)}$ such that $f(x^{(0)}) > 0$, it follows that $f(x^{(t)}) > 0$ for every t. One should start from a random initial value, $x^{(0)}$, and run the algorithm for many iterations until the initial state is forgotten. These discarded samples are known as "burn in." The remaining set of accepted values represents a sample from the stationary distribution.

In the present work, it is suspected from observations that the resulting mass distribution should be a segmented power-law form. For this, we chose the target density as a truncated normal with probability density function (pdf)

$$f(x) = k\frac{1}{\sigma\sqrt{2\pi}}e^{-\frac{x^2}{2\sigma^2}},\ a < x < d, \tag{9}$$

where $k = \frac{1}{\Phi(d/\sigma) - \Phi(a/\sigma)}$,

$$\Phi(t) = \int_{-\infty}^{t} \frac{1}{\sqrt{2\pi}} e^{-x^2/2} dx,$$

and the proposal density as a truncated Pareto with pdf

$$q(y|x) = \frac{\alpha\beta^{\alpha} y^{-\alpha-1}}{1-(\beta/\nu)^{\alpha}},\ \beta < y < \nu. \quad (10)$$

Here, the proposal density does not depend on x. Such a generalization is known as the Independence Chain Metropolis–Hastings algorithm, which is applicable when some a priori knowledge is available regarding the distribution from which one must simulate. In the present study, the appropriate choices of the constants (population parameters) in Equations (9) and (10) are $a = 0.01\,M_{\odot}$, $d = 150\,M_{\odot}$, $\alpha = 1.3$, $\beta = 0.01$, $\nu = 150$, and $\sigma = 10$.

4. RESULTS AND DISCUSSION

4.1. Initial Values of the Parameters

To generate mass distribution as a result of random fragmentation, it is necessary to choose some of the parameters involved in Equations (1)–(4). These are λ, t_1, m_f, and n.

Murray & Lin (1989a, 1989b) have shown that thermal instability in a protoglobular cluster cloud is comparable to the cooling timescale τ_c, where $\tau_c = \frac{3}{2}\frac{kT}{n\Lambda(x,t)}$. For a cloud of mass $1.6 \times 10^6\,M_{\odot}$ and density $n = 270\ \mathrm{cm}^{-3}$, $\tau_c = 0.9\tau_d$, τ_d being the dynamical time. As a result, $\tau_c < \tau_d$. They found that for such a cloud, after 1.58×10^{13} s ($\sim\tau_c$), density fluctuation $\frac{\delta\rho}{\rho}$ increased by a factor of two, and this led to the formation of a cold, dense shell. The timescale for gravitational instability of such a shell drops below this value for $(\rho/m_{\mathrm{H}})_{\mathrm{shell}} \geqslant 1231\ \mathrm{cm}^{-3}$, so the entire process of fragmentation occurs on a timescale much shorter than τ_d, i.e., $\tau_c + \tau_g \leqslant \tau_d$. Since the number densities of molecular clouds vary from 10^4–10^5 (Bally et al. 1987, 1988), the entire time of fragmentation is much less than their dynamical time (Murray & Lin 1989a, 1989b). For a number density in the above range, the dynamical time is on the order of 10^5–10^6 years. Accordingly, the time of fragmentation is chosen between 10^5 and 10^6 years. Because the mass of a YMC is on the order of $10^4\,M_{\odot}$–$10^6\,M_{\odot}$, following Equation (5), $n \sim 1.75$–3 for $N_F \sim 10^3$–10^4. We chose $n = 3$ as a representative value. For the above values, $t_1 \sim \bar{t} \sim 10^5$ years, and hence $\hat{\lambda} > 10^{-5}$. We chose $\hat{\lambda} \sim 10^{-5}$. Several authors (Lada et al. 1984; Elmegreen & Clemens 1985; Verschueren 1990) derived the critical efficiency for isothermal clouds to be 0.29 at $s = 0$ and 0.5 at $s = 1$, where s is the ratio of stellar velocity dispersion to the virial. In the present situation, both values are used as extreme cases. The minimum and maximum masses of fragments were chosen as $0.01\,M_{\odot}$ and $150\,M_{\odot}$, respectively (Zinnecker & Yorke 2007).

The other structural parameters are r_c, $r_{\max}$, $m_{\min}$, and $m_{\max}$. Hunter et al. (1995), Mackey & Gilmore (2003), McLaughlin & van der Marel (2005), Anderson et al. (2009), Vansevičius et al. (2009), Barmby et al. (2009), and Perina et al. (2009) observed several YMCs in the Large Magellanic Cloud (LMC), M31, NGC 6822, and Small Magellanic Cloud. They estimated the values of r_c and virial radius r_{vir} to lie between 1–2 pc and 8–15 pc, respectively, in most cases. Hence, from the above ranges, we took the representative values of r_c and $r_{\max}(\sim r_{\mathrm{vir}})$ as 1.5 pc and 15 pc, respectively. The minimum mass as a result of fragmentation is on the order of $0.01\,M_{\odot}$ or less (Silk 1977; Kanjilal & Basu 1992). The maximum mass of a star in a cluster found so far is on the order of $\sim 10^{-2}\,M_{\odot}$ (Faustini et al. 2009; Martins et al. 2005; Maschberger & Clarke 2008; Parker & Goodwin 2007; Elmegreen 2006). Thus, for $m_{\min}$ and $m_{\max}$, values $\geqslant 0.01\,M_{\odot}$ and $\leqslant 150\,M_{\odot}$ were chosen for convenience. For values of b, the different projected distances from core to envelope were chosen to see the effect of mass segregation from the observational aspect, taking opacity into consideration. While modeling a spherical YMC, the total number of fragments, n_T, chosen was 10,000. The results did not vary with the choice of n_T. The different values of the parameters are listed in Table 1. Here, we note that, although in the EFF model the value of γ lies between 2 and 3, we also used other values of γ from the observed parameters of YMCs by various authors (Zwart et al. 2010 and references therein), as mentioned above.

Table 1
Values of the Various Parameters Used

Parameter	Value
λ	$>10^{-5}$
t_1(years)	$\sim 10^5$
$m_f(M_{\odot})$	$10^4, 5\times10^4, 10^5, 5\times10^5$
n	3
ϵ(%)	0.29, 0.5
b (pc)	1, 1.5, 2, 3, 5, 7, 12
r_c(pc)	1.5
$r_{\max}$(pc)	15
γ	1–3
$m_{\min}(M_{\odot})$	0.01–0.04
$m_{\max}(M_{\odot})$	$\leqslant$150
A, δ	Determined from given conditions
n_T	10,000 within each cluster when modeled as a sphere; any random number during MCMC
$x^{(0)}$	Any random number between 0 and 1
$a(M_{\odot})$	0.01
$d(M_{\odot})$	150
α	1.3
$\beta(M_{\odot})$	0.01
$\nu(M_{\odot})$	150
σ	10

4.2. Mass Distribution as a Result of Random Fragmentation

The resulting mass spectra, generated using Equations (1)–(4) and the Metropolis–Hastings algorithm, are fitted by segmented power laws in different mass regimes and are shown in Table 2 with maximum ($m_{\max}$), minimum ($m_{\min}$), and critical mass (m_c), as well as the corresponding errors for each simulation. The errors are computed by running each simulation many times. It is clear from Table 2 that there are no correlations of critical mass, maximum mass, and mass functions with cloud mass. Considering the existence of a correlation between the maximum mass of a star and the mass of its parent cloud if any, poses a separate constraint on star formation history in clouds of various masses. If the IMF of several constituents in any galaxy is integrated, we get what is called the integrated galactic initial mass function (IGIMF). According to various authors (Bruzal & Charlot 2003; Larson 2006; Weidner & Kroupa 2007; Weidner et al. 2010), low-mass clouds do not have enough mass to form high-mass stars. This only happens if the stars derive their masses from their surroundings, which is actually the case. On the other hand, in massive clouds, once high-mass stars form, their ionizing radiation effectively removes any remaining gas (Weidner & Kroupa 2006), thus stopping the formation of low-mass stars. This leads to a positive correlation between the maximum mass of a star and its parent cloud's mass. This fact is reflected in some observations of clouds of masses in the

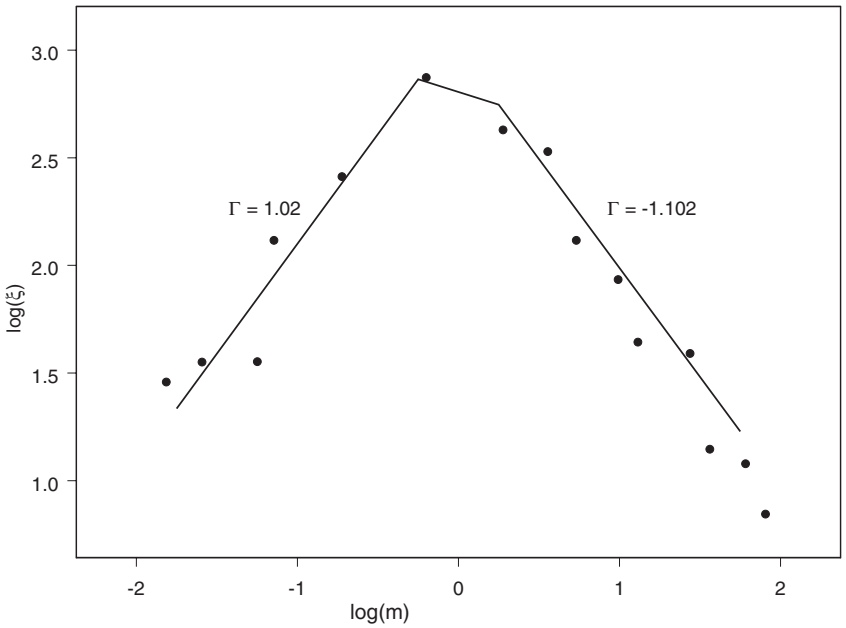

Figure 2. Segmented power-law fit at $b = 3$ pc for a YMC of mass $m_f = 5 \times 10^4\ M_\odot$, with simulated values (solid circles).

Table 2
Segmented Power-law Fit under Various Initial Conditions

m_f	ϵ	n_T	$m_{\rm min} \leqslant m \leqslant m_c$		$m_c \leqslant m \leqslant m_{\rm max}$		$m_{\rm min}$	$m_{\rm max}$	m_c
($M_\odot$)			($M_\odot$)		($M_\odot$)		($M_\odot$)	($M_\odot$)	($M_\odot$)
			Γ	α	Γ	α			
10^4	0.29	3365	1.132 ± 0.051	-0.132	-1.15 ± 0.31	2.15	0.0103 ± 0.00031	95.15 ± 42.32	-0.333 ± 0.015
	0.5	8075	1.084 ± 0.08	-0.084	-1.38 ± 0.94	2.38	0.0100 ± 0.00035	111.59 ± 29.29	-0.350 ± 0.027
5×10^4	0.29	29159	1.312 ± 0.014	-0.312	-1.49 ± 0.18	2.49	0.0100 ± 0.00037	143.51 ± 1.76	-0.559 ± 0.011
	0.5	46854	1.087 ± 0.075	-0.087	-1.60 ± 0.21	2.60	0.0100 ± 0.00016	142.98 ± 2.57	-0.333 ± 0.024
10^5	0.29	46435	1.192 ± 0.022	-0.192	-1.44 ± 0.27	2.44	0.0101 ± 0.00011	131.12 ± 21.09	-0.405 ± 0.030
	0.5	62762	1.222 ± 0.011	-0.222	-1.34 ± 0.24	2.34	0.0100 ± 0.00023	139.85 ± 22.84	-0.431 ± 0.032
5×10^5	0.29	52429	1.147 ± 0.051	-0.147	-1.52 ± 0.18	2.52	0.0100 ± 0.00036	128.03 ± 29.98	-0.346 ± 0.027
	0.5	69363	1.23 ± 0.010	-0.23	-1.38 ± 0.30	2.38	0.0100 ± 0.00023	114.02 ± 31.23	-0.355 ± 0.029

Note. The acceptance of a null hypothesis is within a 95% level of significance in each fit (i.e., $p \gg 0.05$).

range 10–$10^6\ M_\odot$ (Weidner et al. 2010 and references therein). The above phenomenon is supported by models based on sorted sampling. Thus, as a result, the IGIMF becomes steeper than the IMF in a region where the star formation rate (SFR) is low, producing no massive stars, e.g., dwarf galaxies, but the IGIMF is almost identical to the IMF in regions of high SFR that produce sufficient massive stars, e.g., giant galaxies. In contrast, the recent compilations by Maschberger & Clarke (2008) and Parker & Goodwin (2007) included several examples of low-mass clusters containing high-mass stars. Corbelli et al. (2009) found that in YMCs of M33, masses of most massive stars are not strictly limited by the cluster's mass. They noted that previous observational studies did not include massive stars surrounded by low-N clusters. Moreover, unresolved binaries play an important role. Elmegreen (2006) argued that clusters are built stochastically: the large amount of molecular gas present in the star formation region allows high-mass stars to form even in a low-SFR region, i.e., the entire range of masses ($0.01\ M_\odot$ to $150\ M_\odot$) is possible even in a low-SFR region, and as a result the IMF and IGIMF become identical. This phenomenon is supported by a model based on random sampling (Elmegreen 2006). Furthermore, previous observations included very small numbers of YMCs ($\sim 10^4$–$10^6\ M_\odot$), for which any such correlation is difficult to predict, so a more robust physical explanation can be drawn only if there are sufficient observations of the entire mass range of molecular clouds, excluding all biases of the previous observations discussed above. The constancy of the critical mass ($\sim m_c$) might be due to the later phase of slowly rising temperatures which happens as a result of coupling between gas and dust (Larson 2006). The mass function is much shallower in the low-mass regime ($m_{\rm min} < m < m_c$) and much steeper, in most cases, in the high-mass regime ($m_c < m < m_{\rm max}$) compared to the Salpeter index. The value of Γ in the second row of Table 2 is not very convincing due to its high error. The logarithm of the critical mass is also somewhat larger than that found in the observations (Moraux et al. 2007; Elmegreen et al. 2008): $-0.5\ M_\odot$. When these mass functions are considered at different distances (r_i, $i = 1, 2...,$ max) from the cluster center, with $m_{\rm min}$ varying according to Equation (6) and cumulative mass functions computed at different projected distances (two-dimensional), some interesting features emerge (Table 3). The logarithm of the characteristic mass is reduced to $-0.5\ M_\odot$ in most cases. Moreover, the mass functions resemble the observed ones when the projected distance is close to the

Table 3
Segmented Power-law Fit at Different Projected Distances under Various Initial Conditions

m_f	r_c	γ	$r_{\max}$	b	ϵ	$m_{\max}$	$\log m_c$	$m_{\min} \leqslant m \leqslant m_c$		$m_c \leqslant m \leqslant m_{\max}$	
($M_\odot$)	(pc)		(pc)	(pc)		($M_\odot$)	($M_\odot$)	($M_\odot$)		($M_\odot$)	
								Γ	α	Γ	α
10^4	1.5	2.6	15	1	0.5	111.59 ± 29.29	-0.552 ± 0.092	1.03 ± 0.21	-0.03	-0.802 ± 0.15	1.802
5×10^4						142.98 ± 2.57	-0.62 ± 0.037	1.19 ± 0.35	-0.19	-0.793 ± 0.27	1.793
10^5						139.85 ± 22.84	-0.65 ± 0.14	1.04 ± 0.31	-0.04	-0.735 ± 0.19	2.735
5×10^5						114.02 ± 31.03	-0.59 ± 0.048	1.06 ± 0.16	-0.06	-0.711 ± 105	1.711
10^4				1.5		111.59 ± 29.29	-0.553 ± 0.140	1.04 ± 0.25	-0.04	-0.839 ± 0.17	1.839
5×10^4						142.98 ± 2.57	-0.53 ± 0.092	1.18 ± 0.22	-0.18	-0.805 ± 0.39	1.805
10^5						139.85 ± 22.84	-0.61 ± 0.051	1.11 ± 0.17	-0.11	-0.790 ± 0.255	1.790
5×10^5						114.02 ± 31.03	-0.59 ± 0.068	1.18 ± 0.092	-0.18	-0.739 ± 0.18	1.739
10^4				2		111.59 ± 29.29	-0.58 ± 0.035	1.05 ± 0.18	-0.05	-0.854 ± 0.12	1.854
5×10^4						142.98 ± 2.57	-0.61 ± 0.041	1.12 ± 0.22	-0.12	-0.829 ± 0.39	1.829
10^5						139.85 ± 22.84	-0.67 ± 0.018	1.07 ± 0.25	-0.07	-0.831 ± 0.23	1.831
5×10^5						114.02 ± 31.03	-0.60 ± 0.058	1.12 ± 0.11	-0.12	-0.775 ± 0.09	1.775
10^4				3		111.59 ± 29.29	-0.533 ± 0.071	1.02 ± 0.05	-0.02	-1.01 ± 0.28	2.012
5×10^4						142.98 ± 2.57	-0.653 ± 0.05	1.07 ± 0.083	-0.07	-1.105 ± 0.26	2.105
10^5						139.85 ± 22.84	-0.505 ± 0.048	1.05 ± 0.06	-0.05	-0.968 ± 0.26	1.968
5×10^5						114.02 ± 31.03	-0.676 ± 0.06	1.08 ± 0.12	-0.08	-0.827 ± 0.40	1.827
10^4				5		111.59 ± 29.29	-0.533 ± 0.019	1.59 ± 0.087	-0.59	-1.07 ± 0.31	2.07
5×10^4						142.98 ± 2.57	-0.505 ± 0.037	1.05 ± 0.106	-0.05	-1.61 ± 0.29	2.61
10^5						139.85 ± 22.84	-0.554 ± 0.013	1.46 ± 0.065	-0.46	-1.02 ± 0.05	2.02
5×10^5						114.02 ± 31.03	-0.512 ± 0.04	1.05 ± 0.036	-0.05	-1.16 ± 0.17	2.16
10^4				7		111.59 ± 29.29	-0.642 ± 0.077	1.26 ± 0.101	-0.26	-1.43 ± 0.33	2.43
5×10^4						142.98 ± 2.57	-0.685 ± 0.082	1.4 ± 0.06	-0.4	-1.56 ± 0.26	2.56
10^5						139.85 ± 22.84	-0.573 ± 0.02	1.3 ± 0.28	-0.3	-1.47 ± 0.30	2.47
5×10^5						114.02 ± 31.03	-0.586 ± 0.094	1.13 ± 0.074	-0.13	-1.49 ± 0.28	2.49
10^4				12		111.59 ± 29.29	-0.65 ± 0.052	1.29 ± 0.082	-0.29	-1.53 ± 0.304	2.53
5×10^4						142.98 ± 2.57	-0.63 ± 0.091	1.31 ± 0.190	-0.31	-1.65 ± 0.064	2.55
10^5						139.85 ± 22.84	-0.58 ± 0.029	1.42 ± 0.057	-0.42	-1.71 ± 0.278	2.71
5×10^5						114.02 ± 31.03	-0.59 ± 0.061	1.45 ± 0.091	-0.45	-1.86 ± 0.055	2.86

Note. The acceptance of a null hypothesis is within a 95% level of significance in each fit (i.e., $p \gg 0.05$).

cluster center (viz., b = 1–3 pc). In Figure 2, the fitted power laws are shown for a cloud of mass $m_f = 10^4\ M_\odot$ and efficiency $\epsilon = 0.5$ at $b = 3$ pc.

For example, in our Galaxy, the Arches cluster, NGC 3603, and Westerlund 1 are the best examples of YMCs observed so far. In the Arches cluster, the mass function varies from $\Gamma \sim -0.65$ to -1.1 ± 0.2 for $1.3\ M_\odot < m < 10\ M_\odot$ (Figer et al. 1999; Espinoza et al. 2009; Stolte et al. 2002; Kim et al. 2006). Its visual mass, age, and central density are $10^{4.3}\ M_\odot$, 2–4 Myr, and $2 \times 10^5\ M_\odot\ \mathrm{pc}^{-3}$ (Figer et al. 1999). In Table 2, for b = 1–3 pc, the value of Γ for $m_f \sim 10^4\ M_\odot$ varies from -0.802 ± 0.15 to -1.012 ± 0.28 in the high-mass zone ($m_{\max} > m > m_c$), which is compatible with the observed values within the error of precession.

In addition, NGC 3603 is another young (2–3 Myr) and massive cluster in the Galaxy. Using high-resolution VRIHST data, the value of Γ is derived (Sung & Bessell 2004) as -0.9 for the inner 0.6 pc of the cluster over the mass range 1–100 $M_\odot$. From observations of various authors (Sung & Bessell 2004; Stolte et al. 2002; Harayama et al. 2008), the mass function is in the range $\Gamma \sim -0.74$ to -1.3, and its mass is $10^{4.1}\ M_\odot \sim 10^4\ M_\odot$ (Zwart et al. 2010). This is also consistent with the previously stated value of Γ in Table 3.

The observed IMF of Westerlund 1 (Brandner et al. 2008) is $\Gamma = 1.3$ for $3.4\ M_\odot < m < 27\ M_\odot$ at $b = 1.5$ pc. The mass of the above YMC is $10^{4.5}\ M_\odot \sim 3 \times 10^4\ M_\odot$ (Zwart et al. 2010). In Table 3 at b = 1–3 pc, $m_f = 5 \times 10^4\ M_\odot$ and γ varies from -0.793 ± 0.27 to -1.105 ± 0.26, which is also consistent with observations within the error limit.

In all the above observations, the authors found a strong signature of mass segregation, which is evident in Table 3 as one moves to a larger projected distance from the cluster center (e.g., for Westerlund 1, the mass function becomes steeper, i.e., Γ varies from -1.4 to -1.7 radially from 2–3 pc (Brandner et al. 2008), which is almost consistent with Table 3, where for $m_f \sim 5 \times 10^4\ M_\odot$, Γ changes from -1.1 to -1.61 as b increases from 3 to 5 pc).

The above results are consistent with previous studies carried out by Goodwin & Kroupa (2005, 2007) and Duchêne et al. (2007). They carried out numerical simulations and found that nearly all stars form in binary or triple systems, and metallicity, via its role in cooling which imposes an opacity limit on fragmentation, is responsible for producing binary systems (Bate 2005; Goodwin & Kroupa 2007). These high binary fractions affect mass segregation early.

Finally, for some observed YMCs (Zwart et al. 2010), fragmentation was considered by taking m_f as their dynamical masses and r_c and γ from the above work. The fitted power laws and the maximum, minimum, and critical masses are listed in Table 4. The power laws fitted at projected distances from b = 1 pc to 12 pc and critical masses are shown in Table 5. When the values of dynamical masses and γ are not given, they are taken as $10^5\ M_\odot$ and 1.5 pc, respectively, by default. Similar to the previous results (viz., Table 3), the logarithm of critical masses

Table 4
Same as Table 2 but for Observed YMCs with $\epsilon = 0.5$

Name	m_f	n_T	$m_{\rm min} \leqslant m \leqslant m_c$		$m_c \leqslant m \leqslant m_{\rm max}$		$m_{\rm min}$	$m_{\rm max}$	m_c
Reference	$(M_\odot)$		$(M_\odot)$		$(M_\odot)$		$(M_\odot)$	$(M_\odot)$	$(M_\odot)$
			Γ	α	Γ	α			
NGC[1,2] 330	$10^{5.8}$	85627	1.034 ± 0.061	-0.034	-1.27 ± 0.132	2.27	0.0126 ± 0.00078	132.41 ± 8.87	-0.23 ± 0.13
M31[3] (Vdb0)	10^5	72364	1.235 ± 0.040	-0.23	-1.45 ± 0.34	2.45	0.01 ± 0.0019	139.85 ± 12.23	-0.38 ± 0.15
M31[4] (B257D)	10^5	72399	1.231 ± 0.018	-0.23	-1.42 ± 0.19	2.42	0.01 ± 0.00052	138.28 ± 15.60	-0.38 ± 0.21
LMC[1,2] (NGC 2164)	$10^{5.2}$	75774	1.252 ± 0.028	-0.252	-1.13 ± 0.25	2.13	0.01 ± 0.00039	141.08 ± 8.02	-0.47 ± 0.15
LMC[1,2] (NGC 2214)	$10^{5.4}$	82640	1.239 ± 0.022	-0.239	-1.15 ± 0.157	2.15	0.01 ± 0.0028	140.33 ± 3.44	-0.48 ± 0.12
NGC 4038($S2_3$)[5]	$10^{5.4}$	88307	1.215 ± 0.034	-0.215	-1.13 ± 0.164	2.13	0.01 ± 0.0024	123.01 ± 13.8	-0.18 ± 0.048
NGC 4038($S1_5$)[5]	10^5.6	87158	1.215 ± 0.056	-0.215	-1.19 ± 0.137	2.19	0.01 ± 0.00067	113.88 ± 21.35	-0.18 ± 0.081
NGC 4038($S2_1$)[5]	10^6.0	90658	1.194 ± 0.055	-0.194	-1.22 ± 0.20	2.22	0.01 ± 0.00035	133.37 ± 11.06	-0.13 ± 0.02

References. (1) Mackey & Gilmore 2003; (2) McLaughlin & van der Marel 2005; (3) Perina et al. 2009; (4) Barmby et al. 2009; (5) Mengel et al. 2008.

Table 5
Same as Table 3 but for Observed YMCs with $\epsilon = 0.5$ and $r_{\rm max} = 15$ pc

Name	m_f	r_c	γ	b	$m_{\rm max}$	$\log m_c$	$m_{\rm min} \leqslant m \leqslant m_c$		$m_c \leqslant m \leqslant m_{\rm max}$	
	$(M_\odot)$	(pc)		(pc)	$(M_\odot)$	$(M_\odot)$	$(M_\odot)$		$(M_\odot)$	
							Γ	α	Γ	α
NGC 330	$10^{5.8}$	2.61	2.58	1	132.41 ± 8.87	-0.61 ± 0.02	1.10 ± 0.19	-0.10	-1.20 ± 0.19	2.20
				1.5		-0.59 ± 0.017	1.11 ± 0.08	-0.11	-1.28 ± 0.21	2.28
				2		-0.60 ± 0.021	1.12 ± 0.05	-0.12	-1.49 ± 0.02	2.49
				12		-0.64 ± 0.082	1.32 ± 0.14	-0.32	-1.73 ± 0.28	2.73
M31 Vdb0	10^5	1.40	1.5	1	139.85 ± 12.23	-0.66 ± 0.05	1.28 ± 0.27	-0.28	-1.15 ± 0.02	2.15
				1.5		-0.62 ± 0.031	1.19 ± 0.13	-0.19	-1.21 ± 0.057	2.21
				2		-0.61 ± 0.035	1.12 ± 0.021	-0.12	-1.33 ± 0.06	2.33
				12		-0.58 ± 0.17	1.33 ± 0.082	-0.33	-1.43 ± 0.39	2.43
M31 B2570	10^5	3.2	1.5	1	138.28 ± 15.6	-0.58 ± 0.028	1.07 ± 0.31	-0.07	-1.28 ± 0.58	2.28
				1.5		-0.55 ± 0.014	1.15 ± 0.12	-0.15	-1.52 ± 0.11	2.52
				2		-0.57 ± 0.061	1.02 ± 0.06	-0.02	-1.53 ± 0.12	2.53
				12		-0.59 ± 0.091	1.28 ± 0.11	-0.28	-1.77 ± 0.092	2.77
LMC NGC 2164	$10^{5.2}$	1.91	2.96	1	141.08 ± 8.02	-0.64 ± 0.015	1.04 ± 0.62	-0.04	-1.13 ± 0.34	2.13
				1.5		-0.62 ± 0.037	1.12 ± 0.22	-0.12	-1.21 ± 0.092	2.21
				2		-0.58 ± 0.028	1.25 ± 0.032	-0.25	-1.25 ± 0.051	2.25
				12		-0.60 ± 0.053	1.05 ± 0.091	-0.05	-1.27 ± 0.348	2.27
LMC NGC 2214	$10^{5.4}$	2.14	2.26	1	140.33 ± 3.44	-0.63 ± 0.018	1.30 ± 0.33	-0.30	-1.12 ± 0.33	2.12
				1.5		-0.58 ± 0.024	1.09 ± 0.302	-0.09	-1.18 ± 0.31	2.18
				2		-0.60 ± 0.028	1.01 ± 0.05	-0.01	-1.28 ± 0.02	2.28
				12		-0.64 ± 0.082	1.18 ± 0.032	-0.18	-1.55 ± 0.27	2.55
NGC 4038$S2_3$	$10^{5.4}$	0.60	1.5	1	123.01 ± 13.8	-0.59 ± 0.036	1.08 ± 0.25	-0.08	-1.12 ± 0.29	2.12
				1.5		-0.61 ± 0.055	1.22 ± 0.073	-0.22	-1.35 ± 0.28	2.35
				2		-0.63 ± 0.011	1.25 ± 0.06	-0.25	-1.43 ± 0.05	2.43
				12		-0.57 ± 0.071	1.06 ± 0.091	-0.06	-1.62 ± 0.29	2.62
NGC 4038$S1_5$	$10^{5.6}$	1.35	1.5	1	113.88 ± 21.38	-0.56 ± 0.18	1.12 ± 0.36	-0.12	-1.37 ± 0.19	2.37
				1.5		-0.57 ± 0.016	1.14 ± 0.02	-0.14	-1.42 ± 0.189	2.42
				2		-0.58 ± 0.062	1.15 ± 0.017	-0.15	-1.57 ± 0.046	2.57
				12		-0.60 ± 0.087	1.18 ± 0.15	-0.18	-1.69 ± 0.47	2.69
NGC 4038$S2_1$	$10^{6.0}$	0.60	1.5	1	133.37 ± 11.06	-0.64 ± 0.061	1.06 ± 0.51	-0.06	-1.04 ± 0.15	2.04
				1.5		-0.60 ± 0.091	1.18 ± 0.11	-0.18	-1.26 ± 0.23	2.26
				2		-0.62 ± 0.028	1.24 ± 0.04	-0.24	-1.49 ± 0.15	2.49
				12		-0.61 ± 0.092	1.27 ± 0.17	-0.27	-1.49 ± 0.102	2.49

at different projected distances (viz., Table 5) clusters around $-0.5\ M_\odot$ within the error limit, and there is strong evidence of mass segregation.

Since different properties of star clusters have been observed by various authors at different projected distances from the cluster center, the cumulative properties are studied at different pro-

jected distances, e.g., cumulative mass functions. The projected distance can vary from 0 to the size of the cluster (viz., $r_{\max}$). Hence, the segmented mass functions are computed near the core as well as the envelope from the observational point of view. It is clear from Tables 3 and 5 that the slopes of the mass functions computed for various initial conditions become steeper as one moves from core to envelope. In the core region, the mass functions resemble a Salpeter mass function, but are much steeper ($\sim$1.7) in the envelope (viz., $b \sim 12$ pc), with mass range $m_c \leqslant m \leqslant m_{\max}$. This is consistent with the observations of LMC star clusters NGC 1805 and NGC 1818 (de Grijs et al. 2002). The steepness of the IMF is interpreted as resulting from the correction for unresolved binaries (Sagar & Richtler 1991) that are considered a single massive star, so the high value of the index is actually an indication of a larger proportion of low-mass stars than massive stars, which is the effect of opacity-limited fragmentation observed at a larger projected distance from the cluster center.

From the above discussion, it is clear that, in the hierarchical fragmentation scenario, the thermal Jeans mass, opacity, and grain cooling are responsible for the mass segregation and critical mass of the fragment (viz., m_c) observed at different projected distances when the fragment masses are generated randomly using an MCMC method. The minimum, maximum, and critical masses of a fragment are independent of cloud mass.

T. C. thanks B. G. Elmegreen for discussions of various aspects at projected distances. The authors are very much grateful to the referee for some constructive suggestions that substantially improved the quality of the paper.

REFERENCES

Allison, R. J., et al. 2009a, MNRAS, 395, 1449
Allison, R. J., et al. 2009b, ApJ, 700, L99
Anderson, M., Zinnecker, H., Moneti, A., McCaughrean, M. J., Brandl, B., Brander, W., Meylan, G., & Hunter, D. 2009, ApJ, 707, 1347
Ascenso, J., Alves, J., & Lago, M. T. V. T. 2009, A&A, 495, 147
Auluck, F. C., & Kothari, D. S. 1965, Z. Astrophys., 63, 9
Bally, J., Stark, A. A., Wilson, W., & Henkel, C. 1987, ApJS, 65, 13
Bally, J., Stark, A. A., Wilson, W., & Henkel, C. 1988, ApJ, 324, 223
Barmby, P., et al. 2009, AJ, 138, 1667
Bate, M. R. 2005, MNRAS, 363, 363
Boyd, D. F. A., & Whitworth, A. P. 2005, A&A, 430, 1059
Brandner, W., Clark, J. S., Stolte, A., Waters, R., Negueruela, I., & Goodwin, S. P. 2008, A&A, 478, 137
Bruzal, G., & Charlot, S. 2003, MNRAS, 344, 1000
Chattopadhyay, A. K., Kanjilal, T., & Basu, B. 2003, Syst. Anal. Modelling Simul., 43, 1697
Chavarría, L., et al. 2009, arXiv:0911.4888v1
Corbelli, E., Verley, S., Elmegreen, B. G., & Giovanardi, C. 2009, A&A, 495, 479
de Grijs, R., Johnson, R. A., Gilmore, G. F., & Frayn, C. M. 2002, MNRAS, 331, 228
Duchêne, G., et al. 2007, in Protostars and Planets V, ed. B. Reipurth, D. Jewitt, & K. Keil (Tucson, AZ: Univ. Arizona Press), 379
Elmegreen, B. G. 1997, ApJ, 486, 944
Elmegreen, B. G. 2006, ApJ, 648, 572
Elmegreen, B. G., & Clemens, C. 1985, ApJ, 294, 523
Elmegreen, B. G., Klessen, R. S., & Wilson, C. D. 2008, ApJ, 681, 365
Elmegreen, B. G., & Mathieu, R. D. 1983, MNRAS, 203, 305
Elson, R. A. W., Fall, S. M., & Freeman, K. C. 1987, ApJ, 323, 54
Er, X. Y., Ziang, Z. B., & Fu, Y. N. 2009, Chin. Astron. Astrophys., 33, 139
Espinoza, P., Selman, F. J., & Melnick, J. 2009, A&A, 501, 563
Faustini, F., Molinari, S., Testi, L., & Brand, J. 2009, A&A, 503, 801
Feller, W. 1980, Phys. Rev., 57, 906
Figer, D. F., Kim, S. S., Morris, M., Serabyn, E., Rich, R. M., & McLean, I. S. 1999, ApJ, 525, 750
Goodwin, S. P., & Kroupa, P. 2005, A&A, 439, 565
Goodwin, S. P., & Kroupa, P. 2007, in Protostars and Planets V, ed. B. Reipurth, D. Jewitt, & K. Keil (Tucson, AZ: Univ. Arizona Press), 133
Harayama, Y., Eisenhauer, F., & Martins, F. 2008, ApJ, 675, 1319
Hodge, P. W. 1961, ApJ, 133, 413
Hunter, D. A., et al. 1995, ApJ, 448, 179
Kanjilal, T., & Basu, B. 1992, Ap&SS, 193, 17
Kim, S. S., Figer, D. F., Kudritzki, R. P., & Najarro, F. 2006, ApJ, 653, L113
Kroupa, P., Tout, C. A., & Gilmore, G. 1993, MNRAS, 262, 545
Lada, C. J., Margulis, M., & Dearborn, D. 1984, ApJ, 285, 141
Larsen, S. S. 2006, in Planets to Cosmology: Essential Science in Hubble's Final Years, ed. M. Livio (Cambridge: Cambridge Univ. Press), 35
Larson, R. B. 1973, MNRAS, 161, 133
Larson, R. B. 2006, RevMexAA, 26, 55
Mackey, A. D., & Gilmore, G. F. 2003, MNRAS, 379, 151
Marsh, K. A., Kirkpatrick, J. D., & Plavchan, P. 2010, ApJ, 709, 158
Martins, F., Schaerer, D., & Hillier, D. J. 2005, A&A, 436, 1049
Maschberger, T., & Clarke, C. J. 2008, MNRAS, 391, 711
McLaughlin, D. E., & van der Marel, R. P. 2005, ApJS, 161, 304
Mengel, S., Lehnert, M. D., Thatte, N. A., Vacca, W. D., Whitmore, B., & Chandar, R. 2008, A&A, 489, 1091
Moeckel, N., & Bonnell, B. I. A. 2009, MNRAS, 396, 1864
Moeckel, N., & Clarke, C. J. 2011, MNRAS, 410, 2799
Moraux, E., Bouvier, J., Stauffer, J. R., Barrado, N. D., & Cuillandre, J. C. 2007, A&A, 471, 499
Moultaka, J., & Pelat, D. 2004, in ASP Conf., Vol. 320, The Neutral ISM in Starburst Galaxies, ed. S. Aalto, S. Huttemeister, & A. Pedlar (San Francisco, CA: ASP), 44
Murray, S. D., & Lin, D. N. C. 1989a, ApJ, 339, 933
Murray, S. D., & Lin, D. N. C. 1989b, ApJ, 346, 155
Parker, R. J., & Goodwin, S. P. 2007, MNRAS, 380, 1271
Pasquato, M., et al. 2009, ApJ, 699, 1511
Perina, S., et al. 2009, A&A, 494, 933
Robert, C. P., & Casella, C. 1998, in Monte Carlo Statistical Methods (Berlin: Springer), 231
Sagar, R., & Richtler, T. 1991, A&A, 250, 324
Salpeter, E. E. 1955, ApJ, 121, 161
Silk, J. 1977, ApJ, 214, 152
Stolte, A., Grebel, E. K., Brandner, W., & Figer, D. F. 2002, A&A, 394, 459
Sung, H., & Bessell, M. S. 2004, AJ, 127, 1014
Vansevičius, V., Kodaira, K., Narbutis, D., Stonkute, R., Bredzius, A., Deveikis, V., & Semionov, D. 2009, ApJ, 703, 1872
Verschueren, W. 1990, A&A, 234, 156
Weidner, C., & Kroupa, P. 2006, MNRAS, 365, 1333
Weidner, C., & Kroupa, P. 2007, MNRAS, 375, 673
Weidner, C., Kroupa, P., & Bonnell, I. A. D. 2010, MNRAS, 401, 275
Wolf, M., & Vadimir, V. 1986, Ap&SS, 128, 229
Wolf, M., & Vanysek, V. 1986, Ap&SS, 128, 229
Zinnecker, H., & Yorke, H. W. 2007, ARA&A, 45, 481
Zwart, S. F. P., McMillan, S. L. W., & Gieles, M. 2010, ARA&A, 48, 431